

# Faraday dispersion function of disk galaxies with axisymmetric global magnetic fields I

HARUYA EGUCHI,<sup>1</sup> MASAKI SUZUKI,<sup>1</sup> YOSHIMITSU MIYASHITA,<sup>1</sup> SHINSUKE IDEGUCHI,<sup>2</sup> AND KEITARO TAKAHASHI<sup>1</sup>

<sup>1</sup>*University of Kumamoto, 2-39-1, Kurokami, Kumamoto 860-8555, Japan*

<sup>2</sup>*Department of Astrophysics/IMAPP, Radboud University Nijmegen, PO Box 9010, NL-6500 GL Nijmegen, the Netherlands*

Submitted to ApJ

## ABSTRACT

Faraday tomography is a novel method to probe 3-dimensional structure of magnetic fields of polarized radio sources. In this paper, we investigate Faraday dispersion function (FDF) of disk galaxies extending a simple analytic model of galactic magnetic fields developed in Ideguchi *et al.* (2017). The model consists of axisymmetric coherent fields and turbulent fields and we consider the effects of inclination, relative amplitude of coherent and turbulent magnetic fields and pitch angle of coherent fields. Our simple model makes it easy to obtain physical interpretation of FDFs and helps understanding observational results. We find FDFs have two peaks when galaxies are observed with non zero inclination. The gap and relative height of two peaks are dependent on the inclination angle and pitch angle but are not affected by relative amplitude of coherent and turbulent magnetic fields so much. These findings give us an important caution that two peaks in observed FDFs do not necessarily imply the presence of two separate radio sources within a beam.

*Keywords:* magnetic field: galaxy— .....

## 1. INTRODUCTION

Magnetic fields play important roles in many of astrophysical systems. In studies on such objects, 3-dimensional structure of magnetic fields is a key to understand the dynamics of magnetized plasma. Faraday tomography is a technique to reconstruct the distribution of magnetic fields of polarized radio sources along the line of sight (LOS) and a combination with 2-dimensional imaging allows us to probe the 3-dimensional structure (Burn 1966; Brentjens & de Bruyn 2005).

A key quantity in Faraday tomography is Faraday depth defined as

$$\phi(x) = K \int_0^x n_e(x') B_{\parallel}(x') dx' \quad [\text{rad m}^{-2}] \quad (1)$$

where  $n_e(x)$  [ $\text{cm}^{-3}$ ],  $B_{\parallel}(x)$  [ $\mu\text{G}$ ] and  $x$  [pc] are the thermal electron density and magnetic fields parallel to the

LOS and the coordinate along the LOS. The coefficient is  $K = 0.81$  when the above units for  $n_e$ ,  $B_{\parallel}$  and  $x$  are adopted. Then, the Faraday dispersion function (FDF), the complex polarization intensity in Faraday depth space, is related to the polarization spectrum as,

$$P(\lambda^2) = \frac{1}{\pi} \int_{-\infty}^{\infty} F(\phi) e^{2i\phi\lambda^2} d\phi. \quad (2)$$

The FDF is the quantity which can be obtained from Faraday tomography and contains information on the LOS distribution of magnetic fields, high-energy electrons which emit polarized radio waves and thermal electrons. Although the distribution which is given by the FDF is in Faraday depth space, rather than physical space, it gives us much more information than the conventional rotation measure (Schnitzeler *et al.* 2007; Govoni *et al.* 2010; Mao *et al.* 2010; Wolleben *et al.* 2010; Akahori *et al.* 2014; Anderson *et al.* 2016; O'Sullivan *et al.* 2018).

However, there are two major difficulties concerning Faraday tomography. The first is the precise reconstruction of the FDF from observed polarization spec-

trum. Although Eq.(2) is mathematically equivalent to Fourier transform, the inverse transformation to obtain the FDF is incomplete because the observational band is limited to a finite range of  $\lambda^2 (> 0)$ . A lot of algorithms have been developed to extract as much information as possible from observed polarization spectrum: RM CLEAN (Heald *et al.* 2009; Miyashita *et al.* 2016), QU fitting (O’Sullivan *et al.* 2012; Miyashita *et al.* 2019) and sparse modeling (Li *et al.* 2011; Andrecut *et al.* 2012; Akiyama *et al.* 2019).

The second one, which is directly related to the current work, is the interpretation of the FDF. As we stated above, the FDF is the distribution of polarized emission in Faraday depth space, not physical space. Thus, the interpretation of the FDF is not straightforward, even if it was reconstructed precisely somehow. In the case of galaxies, previous works have emphasized that the presence of turbulent magnetic fields is important to understand the shape of the FDF (Beck *et al.* 2009; Bell *et al.* 2011; Frick *et al.* 2011; Ideguchi *et al.* 2014). Generally, the turbulent fields induce randomness in the FDF and make the FDF difficult to interpret.

In our previous study (Ideguchi *et al.* 2017), we developed a simple analytic model of disk galaxies with global (coherent) and turbulent (random) magnetic fields. It was found that randomness of the FDF is significantly reduced when the FDFs of areas which are much larger than the typical scale of turbulence are summed over. The resultant FDF reflects the feature of global fields and the statistical properties of turbulence. In this paper, we extend the model of galaxies developed in Ideguchi *et al.* (2017) to consider the effects of inclination of observation, relative amplitude between global and turbulent magnetic fields and pitch angle of global fields.

The structure of this paper is as follows. In section 2, we describe our model of galactic magnetic fields and method to calculate FDFs. The results are given in section 3. Section 4 is devoted to the summary and discussion.

## 2. MODEL OF DISK GALAXIES

### 2.1. Galaxy Model in Ideguchi *et al.* (2017)

In our previous work (Ideguchi *et al.* 2017), we studied the characteristic properties of the FDF of a small portion,  $\sim (100\text{pc})^2$ , of “face-on” spiral galaxies by employing simple models for the magnetic field. For simplicity, we ignored galactic halos (or thick disks) and considered only galactic disk which has a scale height of  $L_{\text{sh}}$  and is filled with the constant thermal electron density,  $n_e$ . As a representative case, we adopted  $L_{\text{sh}} = 1$  kpc and  $n_e = 0.02 \text{ cm}^{-2}$ . The intensity and angle of

polarization is assumed to be constant within the computational domain. The random magnetic field is also assumed, but the emission from it is ignored and only LOS component of it is considered.

The magnetic fields which is parallel with respect to the line of sight (LOS) is decomposed into random and coherent components such that

$$B'_{\parallel} = B'_{\text{rand}} + B'_{\text{coh}}. \quad (3)$$

We assigned the physical quantities described above to cubic cells of size  $L_{\text{cell}}$ , which is adopted as 10 pc as a representative. This is equivalent to make a simple assumption where  $B'_{\text{rand}}$  has a single coherence length. Under these assumptions, we calculated the FDF numerically by stacking up the cells for  $[-L_{\text{sh}}, L_{\text{sh}}]$ . Thus, each LOS includes  $N = 2L_{\text{sh}}/L_{\text{cell}}$  cells, or “layers” since we also considered number of cells in the plane perpendicular to the LOS which corresponds to the observational region. We found that the “shape” of the FDF becomes smooth when multiple LOSs cover a region of  $\gtrsim (10 \text{ coherence length})^2$ .

As the next step, we derived the FDF analytically in the limit of large number of LOSs. We found that the FDF can be expressed as the sum of many Gaussian functions with different means and variances such that

$$F(\phi) \propto \sum_{j=1}^N P_j(\phi), \quad (4)$$

where  $P_j(\phi)$  is the  $j$ th layer’s contribution to the FDF and is expressed as

$$P_j(\phi) = \frac{1}{\sqrt{2\pi j}\sigma_\phi} \exp\left[-\frac{(\phi - j\Delta\phi_{\text{coh}})^2}{2j\sigma_\phi^2}\right]. \quad (5)$$

Here  $\Delta\phi_{\text{coh}} = Kn_e B'_{\text{coh}} L_{\text{cell}}$  shows the slide of the peak location of the emission from each layer in  $\phi$  space due to the coherent field, and  $\sigma_\phi^2 = K^2 n_e^2 \sigma_B^2 L_{\text{cell}}^2$  with  $\langle B'_{\text{rand}}{}^2 \rangle = \sigma_B^2$  shows the variance of emission from each layer in  $\phi$  space due to the random field within the layer. Note that we do not consider the absolute emissivity of radiation and thus the intensity of  $F(\phi)$  is in arbitrary unit, since we only study the shape of  $F(\phi)$ . We also demonstrated that the simulated FDF approaches to the analytical solution as the number of LOSs increases.

### 2.2. Extension of Galaxy Model

In this work, we follow the basic concepts and parameters of the analytical study of our previous work in Ideguchi *et al.* (2017), but extend it by introducing the inclination of the spiral galaxies as well as the pitch angle of the spiral magnetic field, and study how these

additional parameters make an impact on the shape of the FDF. The values of  $n_e = 0.02 \text{ cm}^{-3}$ ,  $L_{\text{sh}} = 1 \text{ kpc}$ , and  $L_{\text{cell}} = 10 \text{ pc}$  follow our previous work. As in Figure 1, we use Cartesian coordinates  $(x, y, z)$ , where the  $x$ - $y$  plane coincides with the galactic midplane with  $z$  penetrating the midplane, and the origin,  $(x, y, z) = (0, 0, 0)$ , being the same as the galactic center. The inclination angle,  $\theta$ , represents the angle between the LOS and  $z$  axis, and is set as 40 degrees as a representative. The LOS is assumed to be always parallel to  $x$ - $z$  plane, and the location of intersection of LOS and galactic plane (at  $z = 0$ ) is defined as  $(x, y) = (\beta, y)$  which is set as  $(0, 200) \text{ pc}$  as a representative (Figure 2).

As the global magnetic field,  $B_{\text{coh}}$ , we assume the concentric magnetic field centered on the galactic center and that it is parallel to the galactic  $(x$ - $y)$  plane. This ring magnetic field is set as  $5 \mu\text{G}$  as a representative. The perpendicular ( $B_{\perp}$ ) and parallel ( $B_{\parallel}$ ) components of  $B_{\text{coh}}$  with respect to the LOS are expressed as

$$B_{\perp}(z_j) = \frac{\sqrt{(z \tan \theta + \beta)^2 + y^2 \cos^2 \theta}}{\sqrt{(z_j \tan \theta + \beta)^2 + y^2}} B_{\text{coh}}, \quad (6)$$

$$B_{\parallel}(z_j) = \frac{y \sin \theta}{\sqrt{(z_j \tan \theta + \beta)^2 + y^2}} B_{\text{coh}}, \quad (7)$$

where

$$z_j = \left( j - \frac{N}{2} \right) L_{\text{cell}} \cos \theta. \quad (8)$$

Here  $N$  is the number of layers (see below). Though we do not consider the coherent (global and uniform) magnetic field which is perpendicular to the galactic plane as was considered in our previous work, we note that the concentric field generates the coherent component which is parallel to the LOS when  $\theta$  is non-zero as in Equation 7.

Regarding the synchrotron radiation, we need to consider the dependence of  $B_{\perp}$  on it since the direction and strength of  $B_{\perp}$  vary with each layer when both of  $\theta$  and  $y$  are non-zero as in Eq. (6), while both of which are assumed to be constant in our previous work. In this paper, for simplicity, we assume that the emissivity of synchrotron radiation is only proportional to  $B_{\perp}^{1.8}$  and ignore the dependence on the Cosmic-ray electron density. The proportion of 1.8 power of  $B_{\perp}$  corresponds to the frequency distribution  $\propto \nu^{-0.8}$ . This is reasonably close to that suggested by observations of the Milky Way (Reich & Reich 1988) and external radio galaxies (Beck *et al.* 1996). In addition, we do not consider the absolute value of emissivity and focus only on the shape of the FDF. Also, we ignore the change of direction of the concentric field within a layer, and assume that it is constant within the layer.

The random magnetic field is also assumed. The polarization from its perpendicular component is ignored also in this study. While the contribution of emission from the random field to  $F(\phi)$  is not trivial, we confirm that it basically affects only to the amplitude of  $F(\phi)$  and hardly affects to the shape of it (Miyashita *et al.* in preparation 2019). Thus, only LOS component of the field,  $B_{\text{rand}}$ , is considered in this work, and it affects to the variance of emission from each layer in  $\phi$  space. As a representative,  $B_{\text{rand}}$  is set as  $1 \mu\text{G}$ , then  $\sigma_B = 1 \mu\text{G}$ .

Under the assumptions described above, the FDF from  $j$ th layer can be expressed using Eq. (5) as

$$P_j(\phi) = \frac{B_{\perp}(z_j)^{1.8}}{\sqrt{2\pi} j \sigma_{\phi}} \exp \left[ -\frac{(\phi - \phi_0(z_j))^2}{2j\sigma_{\phi}^2} \right] \times \exp[2\chi(z_j)], \quad (9)$$

where

$$\phi_0(z_j) = K n_e L_{\text{cell}} \sum_{k=1}^j B_{\parallel}(z_k), \quad (10)$$

$$\chi(z_j) = \cos^{-1} \left[ \frac{z_j \tan \theta + \beta}{\sqrt{(z_j \tan \theta + \beta)^2 + y^2 \cos^2 \theta}} \right], \quad (11)$$

and  $\sigma_{\phi}^2 = K^2 n_e^2 \sigma_B^2 L_{\text{cell}}^2$  with  $\langle B_{\text{rand}}^2 \rangle = \sigma_B^2$ . Since we always consider the region for  $[-L_{\text{sh}}, L_{\text{sh}}]$  through  $z$  axis, the number of layers depends on the inclination angle and is expressed as

$$N = \frac{2L_{\text{sh}}}{L_{\text{cell}} \cos \theta}. \quad (12)$$

Finally,  $F(\phi)$  is calculated using Equation 4 and Eq. (9).

When non-zero pitch angle of spiral field,  $\theta'$ , is considered,  $F(\phi)$  is calculated in the same way by modifying Equation 6, 7 and 11 as

$$B_{\perp}(z_k) = \frac{\sqrt{(z_j \tan \theta + \beta)^2 + y^2 - (y \cos \theta' + (z_j \tan \theta + \beta) \sin \theta')^2 \sin^2 \theta}}{\sqrt{(z_j \tan \theta + \beta)^2 + y^2}} B_{\text{coh}}, \quad (13)$$

$$B_{\parallel}(z_k) = \frac{(y \cos \theta' + (z_j \tan \theta + \beta) \sin \theta') \sin \theta}{\sqrt{(z_j \tan \theta + \beta)^2 + y^2}} B_{\text{coh}}, \quad (14)$$

and

$$\chi'(z_k) = \cos^{-1} \left[ \frac{(z_j \tan \theta + \beta) \cos \theta' - y \sin \theta'}{\sqrt{((z_j \tan \theta + \beta)^2 + y^2) \cos^2 \theta + (y \sin \theta' - (z_j \tan \theta + \beta) \cos \theta')^2 \sin^2 \theta}} \right]. \quad (15)$$

We start with the fiducial model where the turbulent field is assumed to be smaller than the global field for allowing us to simply interpret the results, and later in the next section, we consider the comparable or larger

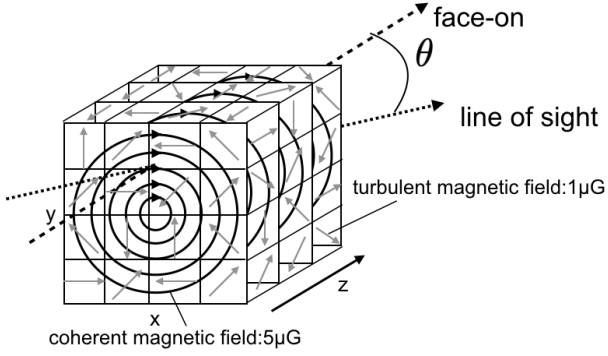


**Figure 1.** Schematic picture of the galactic model used in this paper.

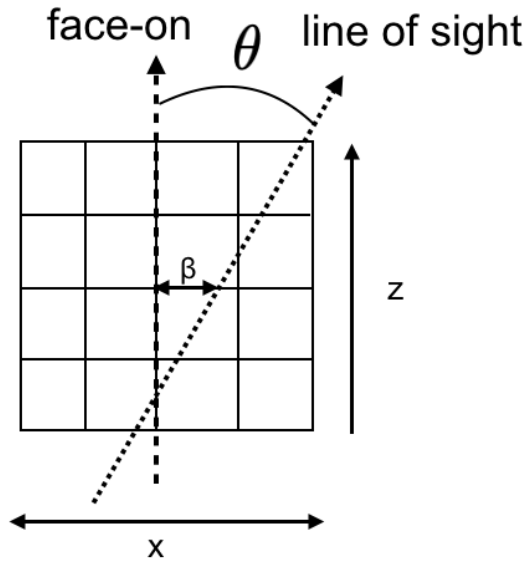


**Figure 2.** This shows the pattern diagram of our galaxy model viewed from above.

turbulent field with respect to the global field whose situation is suggested by observations (Fletcher 2010). The model parameters and their fiducial values used in this paper are summarized in Table 1.

### 3. RESULTS

#### 3.1. basic results

First, let us see the case of  $\theta = 0$  deg (face-on) discussed in Ideguchi *et al.* (2017). The absolute value of the FDF is shown in Fig. 3. As explained in Section 2, the FDF is the sum of contribution from all layers along the line of sight. Because ring fields are perpendicular to the line of sight, only turbulent fields contribute to the parallel component of magnetic fields. In this case, the center of Gaussian function of each layer is located at  $\phi = 0$ , while the width is larger for larger  $j$ . Thus,

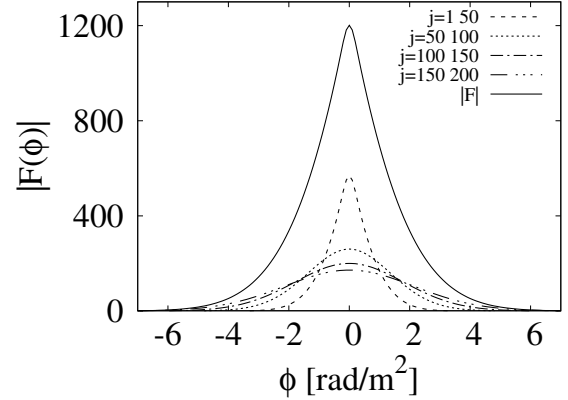


**Figure 3.** Absolute value of Faraday dispersion function for the case with  $\theta = 0$  deg (face-on). Solid line corresponds to the total FDF. Contribution from groups of layers with  $j = 1 - 50, 51 - 100, 101 - 150$  and  $151 - 200$  are also shown.

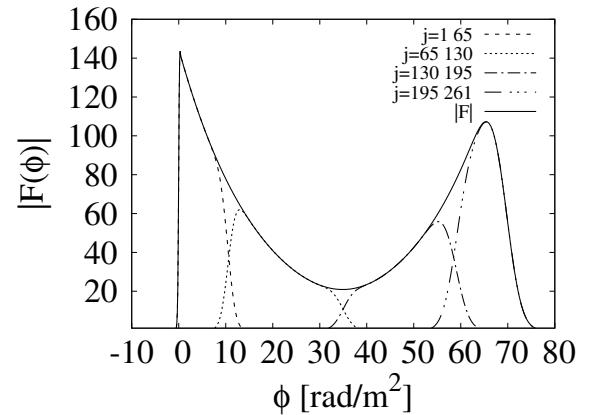


**Figure 4.** Same as Fig. 3 but for inclination  $\theta = 40$  deg.

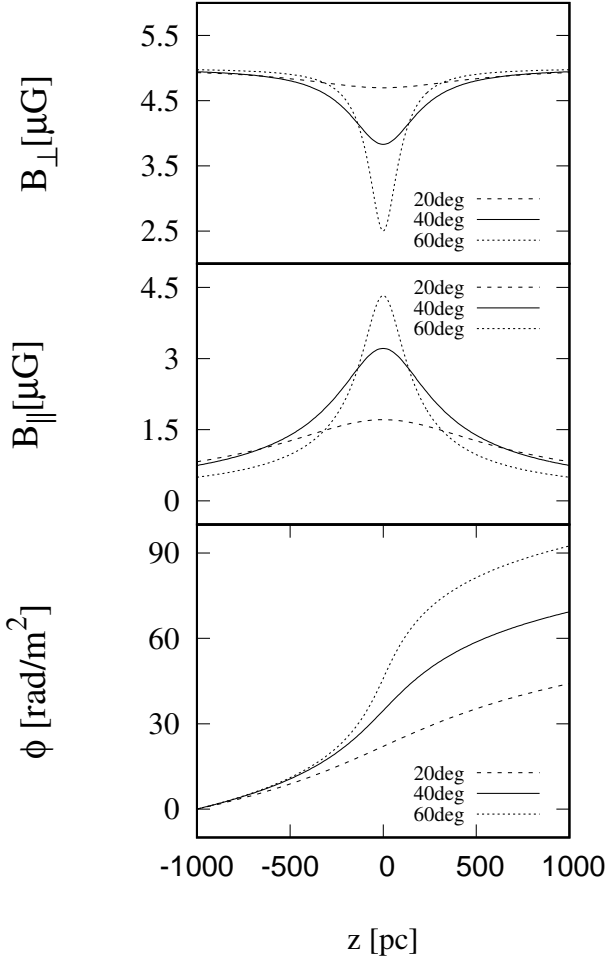
the FDF is the sum of Gaussian functions with the same center ( $\phi = 0$ ) and different widths and is not Gaussian itself. The width of the FDF reflects the magnitude of turbulent magnetic fields. Ideguchi *et al.* (2017) further considered the case with coherent magnetic fields perpendicular to the galactic plane and found that the FDF is skewed.

Fig. 4 represents the FDF with inclination  $\theta = 40$  deg and offset from the galactic center of  $y = 200$  pc and  $\beta = 0$  pc. Two peaks can be seen at  $\phi = 0$  and  $65$  rad/m<sup>2</sup> and the left peak is sharp compared with the other. These features were not seen in the situation considered in Ideguchi *et al.* (2017).

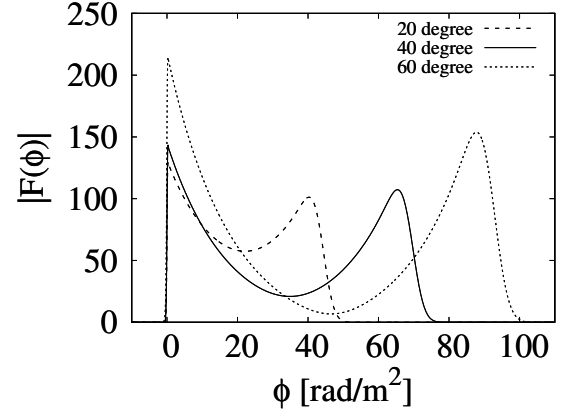
To understand these features, we plot the distribution of magnetic field components and  $\phi(z)$  along the line of sight in Fig. 5. The top panel represents the perpendicular component of coherent fields and it is small around the galactic plane ( $z \sim 0$ ). Because the emissivity of synchrotron radiation is assumed to be proportional to

**Table 1.** Fiducial model parameters

Symbol	Physical Quantity	Fiducial Value
$\theta$	inclination angle	40 deg
$\theta'$	pitch angle	0 deg
$y$	height of LOS	200 pc
$\beta$	intersection of LOS and galactic plane	0 pc
$n_e$	thermal electron density	$0.02 \text{ cm}^{-3}$
$B_{\text{coh}}$	coherent magnetic field	$5 \mu\text{G}$
$B_{\text{ran}}$	standard deviation of turbulent magnetic fields	$1 \mu\text{G}$


**Figure 5.** Distribution of  $B_{\perp}$  (top) and  $B_{\parallel}$  (middle), and Faraday depth (bottom) along a line of sight with different inclination  $\theta = 20, 40$  and  $60$  degree for the fiducial model.

$B_{\perp}^{1,8}$ , the emissivity around the galactic plane is consequently relatively low. On the other hand, the distribution of the parallel component is shown in the middle panel and the resulting Faraday depth is plotted in the bottom panel as a function of  $z$ . Since  $\phi(z)$  is monotonically increasing because  $B_{\parallel} > 0$  everywhere, Gaussian functions move rightward with increasing  $j$ . This can also be seen in Fig. 4, where the contributions from 4


**Figure 6.** Absolute value of Faraday dispersion function for the cases with  $\theta = 20, 40$  and  $60$  deg.

groups of layers are also shown. Thus, we can see that the peak at  $\phi = 0$  is mostly contributed from emission from the near side of the galaxy, while the other is from the far side. The sharpness of the peaks can also be explained by the fact that Gaussian functions of the far side have larger widths.

It should be noted that the dip between the two peaks around  $\phi \sim 35$  corresponds to the galactic plane  $z \sim 0$  (see the bottom panel of Fig. 5). There are two reasons for the existence of the dip. One is that a relatively few number of layers are contributing to the FDF at  $\phi \sim 35$  since  $B_{\parallel}$  is large around  $z \sim 0$  and  $\phi$  is rapidly increasing as can be seen in the middle and bottom panels of Fig. 5. Another reason is that the emissivity is relatively low there as stated above.

Fig. 6 shows the absolute value of the FDF for different inclination angles (20, 40 and 60 deg). As can be seen in the middle panel of Fig. 5,  $B_{\parallel}$  at the galactic plane is larger for a larger inclination angle, while the mutual relation is reversed off the plane. On the other hand, the path length within the galaxy along the line of sight is longer for a larger inclination. Here, note that the horizontal axis of Fig. 5 is  $z$ , rather than the path length. As a result of these factors, Faraday depth

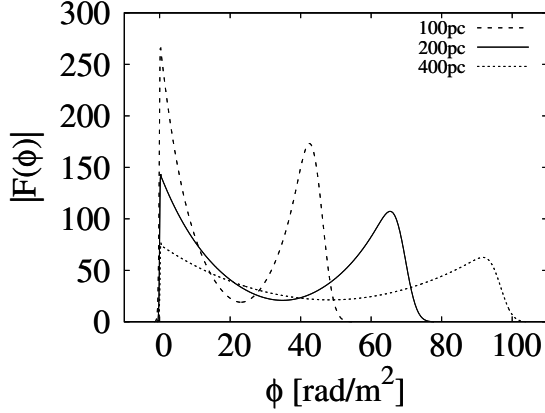


**Figure 7.** Same as Fig. 6 but for  $y = 100, 200$  and  $400$  pc. The inclination angle  $\theta$  is fixed to  $40$  deg.

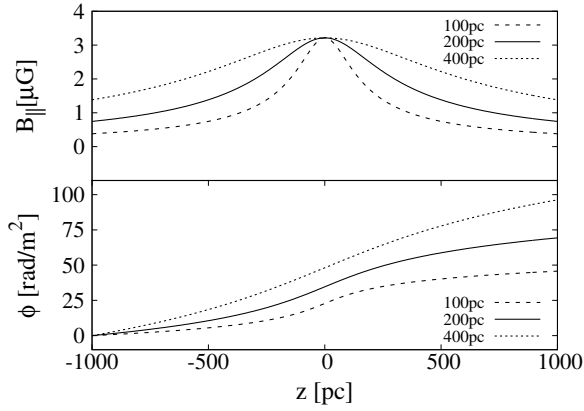


**Figure 8.** Distribution of  $B_{\parallel}$  (Top), and Faraday depth (Bottom) along a line of sight with different offset  $y = 100, 200$  and  $400$  pc. The inclination angle  $\theta$  is fixed to  $40$  deg.

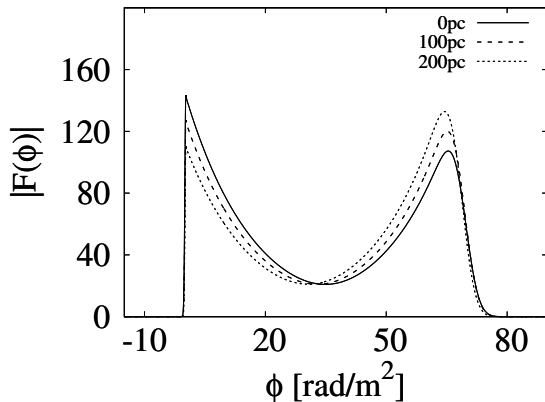


**Figure 9.** FDF distribution in the case of  $\beta = 100, 200$  and  $400$  pc.

turns out to be larger for a larger inclination and, consequently, the gap between the two peaks is larger.

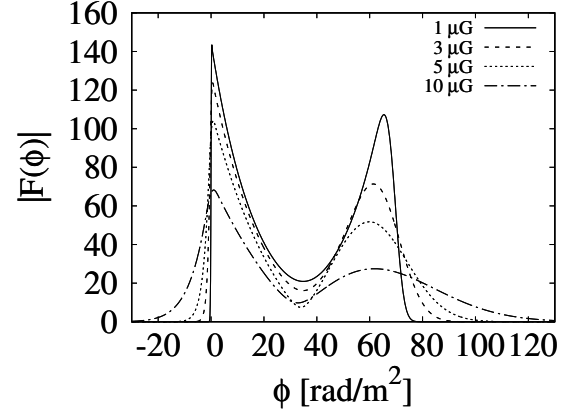


**Figure 10.** Absolute value of the FDFs with turbulent magnetic fields of  $1, 3, 5$  and  $10 \mu\text{G}$ .

Finally, let us see the variation of the FDF when the offset of the line of sight from the galactic center is changed. Fig. 7 shows the absolute value of the FDF for  $y = 100, 200$  and  $400$  pc, fixing  $\theta = 40$  deg and  $\beta = 0$  pc. The distribution of  $B_{\parallel}$  and Faraday depth along the line of sight are shown in Fig. 8. The offset does not affect the maximum value of  $B_{\parallel}$  but its variation is smaller for a larger offset. Thus, Faraday depth grow more rapidly and the gap between the two peaks is larger for a larger offset. On the other hand, significant change cannot be seen in Fig. 9, where  $\beta$  is shifted to  $100, 200$  and  $400$  pc with fixed values of  $y = 200$  pc and  $\theta = 40$  degree.

### 3.2. variant models

In the previous subsection, a simple model of a galaxy was adopted to understand the behavior of the FDF easily. We extend the fiducial model in several ways to consider more variations of observed galaxies.

#### 3.2.1. turbulent magnetic fields

In most galaxies, turbulent magnetic fields are comparable or stronger than coherent fields. In this subsection, we investigate the FDFs varying the amplitude of turbulent fields and fixing that of coherent fields. Fig. 10 shows the absolute value of the FDFs with turbulent magnetic fields of  $1, 3, 5$  and  $10 \mu\text{G}$ . For stronger turbulent fields, the Gaussian function of each layer widens so that the peaks become smooth. On the other hand, the centers of Gaussian functions are unchanged because the magnitude of coherent fields is fixed, so the position of peaks do not change so much either. Thus, these FDFs have most of the features of the FDF of the fiducial model and the discussion given in the previous subsection applies to the current case as well.

#### 3.2.2. pitch angle

Here we consider coherent magnetic fields with pitch angle by rotating the ring field at each position as stated in section 2. Fig. 11 shows the line-of sight distribution of perpendicular and parallel components of magnetic fields and  $\phi(z)$  for pitch angle  $\theta' = 0, 20, 40$  and  $60$  deg with fixed inclination  $\theta = 40$  deg. It is seen that, for non zero pitch angle, the distribution of magnetic fields is not symmetric with respect to the galactic plane ( $z = 0$ ) as opposed to the case with ring fields. The parallel component starts from a negative value and becomes positive at somewhere in the near side ( $z < 0$  pc). The transition point is closer to the galactic plane for a larger pitch angle. Consequently, Faraday depth first decreases from zero, takes the minimum value at the transition point and becomes positive in the end.

Resultant FDFs are shown in Fig. 12. Because Faraday depth becomes negative for non zero pitch angle, the left peak moves to negative  $\phi$  region and is located at the minimum  $\phi$ . Therefore, the Faraday depth of the peak is smaller (larger  $|\phi|$ ) for a larger pitch angle. On the other hand, the right peak has a lower height and is located at a smaller  $\phi$  for a larger pitch angle. This is because only a narrow range of  $z$  contributes to the right peak for a large pitch angle (see the bottom panel of Fig. 11). The magnitude of perpendicular component shown in the top panel of Fig. 11 also affects the peak height, but this factor is very minor. It should be noted that the vertical axis of Fig. 12 is in logarithmic scale, while that of Fig. 5 is in linear scale.

Figs. 13 and 14 are comparison between different inclination angles ( $\theta = 0, 20$  and  $40$  deg) for fixed pitch angle of  $\theta' = 30$  deg. We can see that the effects of non zero pitch angle such as asymmetry of magnetic fields with respect to the galactic plane are more significant for a larger inclination angle.

#### 4. SUMMARY AND DISCUSSION

In this paper, we investigated Faraday dispersion function (FDF) of disk galaxies extending a simple analytic model of galactic magnetic fields developed in Ideguchi *et al.* (2017), which has axisymmetric coherent fields and turbulent fields. We studied the effects of inclination, relative amplitude of coherent and turbulent fields and pitch angle of coherent fields. Our model was rather simple but allowed us to understand the behavior of FDFs. First, we found FDFs have two peaks when galaxies are observed with non zero inclination. The gap and relative height of two peaks are dependent on the inclination angle and pitch angle. The relative amplitude of coherent and turbulent magnetic fields does not affect the qualitative features so much and widens the peaks.

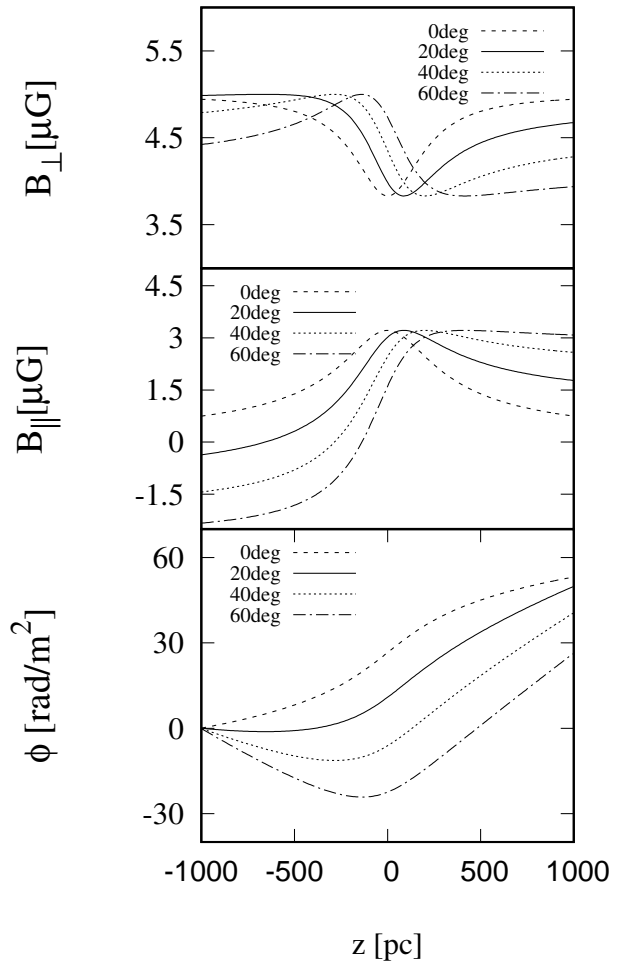


**Figure 11.** Same as Fig. 5 but with pitch angle  $\theta' = 0, 20, 40$  and  $60$  deg and fixed inclination  $\theta = 40$  deg.

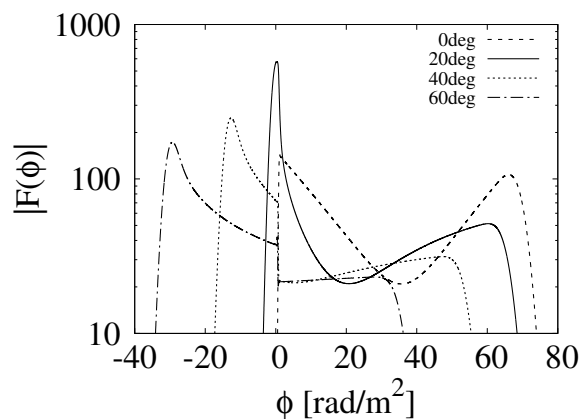


**Figure 12.** Same as Fig. 3 but with pitch angle  $\theta' = 0, 20, 40$  and  $60$  deg and fixed inclination  $\theta = 40$  deg.

It is rather surprising that FDFs exhibit a wide variety of shape just by varying the inclination and pitch angles. Especially, the fact that non zero inclination leads to

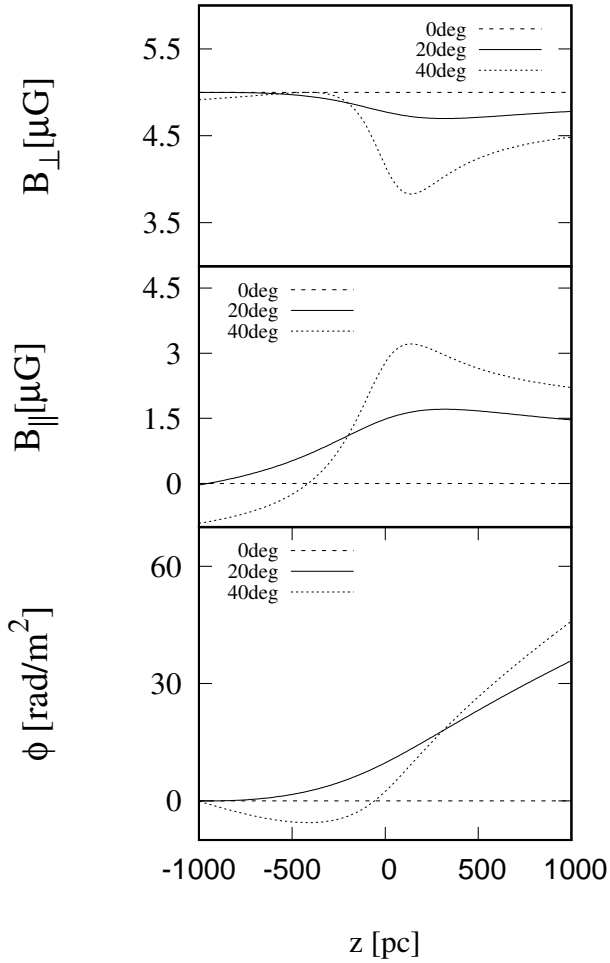


**Figure 13.** Same as Fig. 5 but with inclination  $\theta = 0, 20$  and 40 deg and fixed pitch angle  $\theta' = 30$  deg.

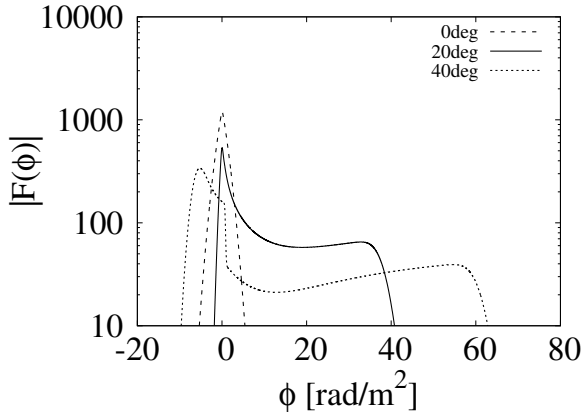


**Figure 14.** Same as Fig. 3 but with inclination  $\theta = 0, 20$  and 40 deg and fixed pitch angle  $\theta' = 30$  deg.

two peaks in the FDF gives us an important caution. In practical observations, emission between the two peaks may not be identified due to thermal and systematic noises. Therefore, one may recognize that the FDF is contributed from two separate radio sources within the beam. Simulations of reconstruction of FDFs studied here with observational errors will be given elsewhere.

Combining Faraday tomography and 2-dimensional imaging, we will be able to obtain Faraday cube, that is, polarization emissivity as a function of Faraday depth and position in the sky. This will allow us probe 3-dimensional structure of galactic magnetic fields, such as topology of global fields and the position dependence of the strength of turbulent fields. Investigation of Faraday cube is also our future work.

#### ACKNOWLEDGEMENT

KT is partially supported by JSPS KAKENHI Grant Numbers JP15H05896, JP16H05999 and JP17H01110, and Bilateral Joint Research Projects of JSPS. YM is supported in part by Grand-in-Aid from JSPS Research Fellow, No. 17J06936.

#### REFERENCES

Akahori, T., Kumazaki, K., Takahashi, K., and Ryu, D.: 2014, *Publications of the Astronomical Society of Japan* **66**, 65.

Akiyama, K., Akahori, T., Miyashita, Y., Ideguchi, S., Yamaguchi, R., Ikeda, S., and Takahashi, K., 2019, submitted to *Astrophys. J.*

- Anderson, C.S., Gaensler, B.M., and Feain, I.J.: 2016, *Astrophys. J.* **825**, 59.
- Andrecut, M., Stil, J. M., & Taylor, A. R. 2012, *AJ*, 143, 33  
1996ARA&A..34..155
- Beck, R., Brandenburg, A., Moss, D., Shukurov, A., Sokoloff, D., 1996, *ARA&A*, 34, 155
- Beck, R. 2009, *ApJ*, 320, 77
- Bell, M. R., Junklewitz, H., & Ensslin, T. A. 2011, *A&A*, 535, A85
- Brentjens, M. A., & de Bruyn, A. G. 2005, *A&A*, 441, 1217
- Burn, B. J. 1966, *MNRAS*, 133, 67
- Fletcher, A., 2010, *ASPC*, 438, 197
- Frick, P., Sokoloff, D., Stepanov, R., & Beck, R. 2011, *MNRAS*, 414, 2540
- Govoni, F., Dolag, K., Murgia, M., Feretti, L., Schindler, S., Giovannini, G., Boschin, W., Vacca, V., and Bonafede, A.: 2010, *Astron. Astroph.* **522**, A105.
- Heald, G., Braun, R., and Edmonds, R.: 2009, *Astron. Astroph.* **503**, 409.
- Ideguchi, S., Tashiro, Y., Akahori, T., Takahashi, K., & Ryu, D. 2014, *Astrophys. J.* **792**, 51.
- Ideguchi, S., Tashiro, Y., Akahori, T., Takahashi, K., and Ryu, D.: 2017, *Astrophys. J.* **843**, 146.
- Li, F., Brown, S., Cornwell, T. J., and de Hoog, F. 2011, *A&A* **531**, A126
- Mao, S.A., Gaensler, B.M., Haverkorn, M., Zweibel, E.G., Madsen, G.J., McClure-Griffiths, N.M., Shukurov, A., and Kronberg, P.P.: 2010, *Astrophys. J.* **714**, 1170.
- Miyashita, Y., Ideguchi, S., Takahashi, K.: 2016, *Publications of the Astronomical Society of Japan* **68**, 44.
- Miyashita, Y., Ideguchi, S., Nakagawa, S., Akahori, T., and Takahashi, K.: 2019, *Monthly Notices of the Royal Astronomical Society* **482**, 2739.
- Miyashita, Y., Ideguchi, S., Takahashi, K., in preparation
- OSullivan, S. P., Brown, S., Robishaw, T., et al. 2012, *MNRAS*, **421**, 3300.
- O’Sullivan, S., Brüggén, M., Van Eck, C., Hardcastle, M., Haverkorn, M., Shimwell, T., Tasse, C., Vacca, V., Horellou, C., and Heald, G.: 2018, *Galaxies* **6**, 126.
- Reich, P., & Reich, W., 1988, *A&AS*, 74, 7
- Schnitzeler, D.H.F.M., Katgert, P., and de Bruyn, A.G.: 2007, *Astron. Astroph.* **471**, L21.
- Wolleben, M., Landecker, T.L., Hovey, G.J., Messing, R., Davison, O.S., House, N.L., Somaratne, K.H.M.S., and Tashev, I.: 2010, *The Astronomical Journal* **139**, 1681.